Brain Tumor Classification Using Ensemble Deep Learning Model With Content Based Medical Image Retrieval

M.Arthi[1]*, Dr.V.P.Eswaramurthy[2]

[1]Research Scholar, Department of Computer Science ,Periyar University Salem-636 011,
Email: arthykvarshana@gmail.com
[2]Assistant professor of Computer Science, Government Arts and Science College, Komarapalayam- 638 183,
Email:eswaramurthy67@gmail.com
*Corresponding Author

Received: 17.07.2024 Revised: 18.08.2024 Accepted: 05.09.2024

ABSTRACT
Brain tumors are among the world's most dangerous causes of death. Magnetic Resonance Imaging (MRI) are non-invasive imaging techniques that neuro radiologists utilize extensively to diagnose Glioma grades. Therapy planning is negatively impacted by the laborious and extremely subjective process of diagnosing brain tumors from radiological imaging, which is vulnerable to intra- and inter-observer variability. If pertinent image graphs are obtained from a large medical image collection, better medical care related to comparable previous situations can be given. Systems for retrieving images based on content are effective tools for handling large datasets. Convolutional Neural Network-based feature extraction techniques can be used in a CBIR system to efficiently automate the categorization and retrieval of comparable pathological images. This research work proposed an ensemble deep learning (DL) based classifications and medical image retrievals for MRI brain tumor images using content-based methods. In the initial stage, content-based image retrieval (CBIR) selects query or template image features and then computes measures of similarity for detecting tumors. During the image pre-processing step, an Enhanced Bilateral Filter (EBF) is used which is an improved version of the bilateral filter used in image processing to preserve edges while reducing noise. Then the image Normalization process is carried out using improved Weibull Cumulative Distribution Function (IWCDF). Following this stage, the tumor portion is identified by applying the Watershed Segmentation method to segment the images. Next, the Enhanced Whale Optimization Algorithm (EWOA) is used to extract features. The enhanced cuckoo search (ICSA) algorithm is then used to carry out the feature selection. At the indexing step, the R*-tree approach is used to improve search efficiency, and Mahalanobis Distance with relevance feedback is used to compute the similarity measure during that phase. Lastly, a model called Ensemble Deep Learning (EDL) is suggested for brain tumor diagnosis. Experiments have used brain MRI data from database of medical images. The suggested approach improves accuracy, recall, and retrieval time.

Keywords: Content-Based Image Retrieval (CBIR) system, preprocessing, Enhanced Bilateral Filter (EBF), WaterShed (WS) method, Enhanced Whale Optimization Algorithm (EWOA), Watershed Segmentation algorithm and Ensemble Deep Learning (EDL).

1. INTRODUCTION

Brain tumors are invasive and pervasive in the small cerebral cavity, making them fundamentally dangerous and perhaps fatal. The death rates resulting from brain tumors are steadily rising [1]. Brain tumors can be classified as benign or malignant based on growths where the former do not spread to adjacent tissue, grow slowly while malignant tumors spread quickly, cause cancer, and infiltrate adjacent organs. Because of the significant differences in their clinical behavior, prognosis, and therapy, brain tumors must be classified accurately. To provide the best possible care for patients, it is essential to distinguish between benign and malignant tumors. A radiologist's visual inspection of brain MR images is necessary for the screening tests that identify brain tumors. However, visual inspection is laborious, subjective, and time-consuming. Computer-aided diagnostic (CAD) systems address these shortcomings and enhance sensitivity of diagnosis by 20–30% in comparison to visual analysis diagnosis [2]. The CAD system includes CBIR, which is a crucial component that helps radiologists diagnose malignancies. Along with diagnostic and treatment information, MRI images of patients collected for diagnosis are stored known as the Image Archiving and Communication System (PACS) [3]. If radiologists are not sure of brain tumors, they can search through the database to locate images that have already been resolved for based

their understanding of related diagnostic disease entities and characteristics of query images are matched [4]. Radiologists can diagnose brain cancers by using case-based reasoning with the use of image retrieval. In PACS, text-based retrieval methods are increasingly often employed. These systems query images using related text from images and keywords from lab reports. Despite the fact that this method allows for a great deal of flexibility in query design, it has a number of limitations, including manual annotations of image descriptions in databases and subjectivity as human perceptions differ [5].Hence, throughout the retrieval process, text retrievals generate mistakes. CBIR, on the other hand, extracts comparable images from the database by analyzing the image's shape, texture, location, and gray level [6] resulting in enhanced CBIR researches.

CBIR approaches [7-8] comprised of many stages: DML, feature extractions (tumor outlines, tumor areas, feature selections, and dimensionality reductions), and pre-processing. In the feature extraction stage, there are two issues. First, it only pays attention to features that are either high-level or low-level. A particular category's content is distributed with inherent irregularity in CE-MRI dataset. Edema, and tumor have significant relationships with surrounding normal tissues. Meningiomas and pituitary tumors have comparable form and are often unrelated to edema, as seen in Figs. 2(a) and (b). Meningiomas are frequently observed near skulls, grey matters, and CSF fluids. Pituitary tumors are found close to sphenoidal sinuses, ocular chiasmas, and internal carotid arteries. Edema typically encircles gliomas, which have different forms, as seen in Figures 2(c) and (d). Second, features such as borders, textures, sizes, and shapes of tumorous patches in magnetic resonance imaging are crucial for distinguishing between various types of brain tumors. Because they use handcrafted features like tumorous region segmentation and outline detection, which require strong prior knowledge including positions or locations of tumorous regions in images, CBIR systems, which are based on traditional machine learning (ML), are not simple tasks and may result in inter- and intra-operator deviations [9]. Hence, feature extraction frameworks that can encode and mix high/low-level information are pertinent.

Recent studies [10] confirmed that previous domain knowledge and manually extracted (handcrafted) features are not required for DL techniques. The feature extraction step of self-learning is embedded by DL. It identifies key characteristics in a self-learning way and requires little or no dataset preparation [11]. One major difficulty for CBIR systems in MRI images is minimizing visual high/low level semantic gaps based on human evaluations. These are crucial to feature extraction approaches for feature representations that include both high-level and low-level data. In order to provide strong discriminative features that bolster viability of suggested CBIR system, CNNs use hierarchical learning for extracting lower level features and high-level domain specific attributes (contents) from feature maps.

These low-level feature maps are built upon and combined by higher layers to create abstract representations that encode and produce both local and global data. Basic structural information, including edges, forms, and textures, are encoded in lower-layer feature maps. Cutting-edge ML techniques were eclipsed by DL. Improved computer vision performance specifically encouraged the use of DL in medical image analyses [12], classifications [13], segmentations [14], fusions [15], computer-based diagnosis and predictions [16], lesions/landmark detections [17], microscopic image assessments [18], and CBIR [19].

However, the performance of these approaches is much below the practical norm, and their development has been progressing slowly in recent years. Furthermore, the process of extracting and selecting features takes a lot of time and varies depending on the item. CNNs, in particular, are types of deep neural networks (DNN) that are extensively employed for changing image categorization tasks and have demonstrated notable performances. This study suggested CBIR and ensemble DL-based classification for MRI brain tumor images. To reduce patient wait times and avoid misdiagnosis, this project aims to build automated diagnostic tools for physicians. This research specifically accomplishes this automation by using patient brain scans to classify different forms of brain tumors. A physician must review many image slices in order to diagnose a patient, delaying more involved diagnosis. With confidence, we will identify the different forms of brain cancer so that doctors may focus on treating patients rather than diagnosing difficult cases.

The rest of this paper is organized as follows: Section 2 investigates recent ML and DL techniques used classifying brain tumors. The suggested technique is presented in Section 3, experimental outcomes and discussions form Section 4 while future work and conclusions are in Section 5.

2. LITERATURE REVIEW

In the second section, many new methods for detecting brain tumors employing sophisticated ML and DL approaches are reviewed.The CBIR technique suggested by Arakeri et al. [20] retrieves comparable MR images in two steps. Using distinction criteria between classes, query images are first categorized as either benign or malignant. The next stage identifies nearly similar images inside projected classes by

using class defining characteristics. A novel indexing which clusters with principle component analysis (PCA) and KD-trees is used as this method integrates subclass characteristics into groups using modified K-means clustering. and independently applies PCA to reduce each cluster's dimensionality to facilitate faster image retrieval.

A KD-tree is then used to index the smaller feature set. Additionally, the suggested CBIR system is strengthened against misalignment that might happen during the gathering of MR images. Their experiments used 820 MRI images of brain tumors where outcomes of their trials validated the practicality of the suggested system's clinical use and its efficacy.

Swati et al [21] offered CBIR where brain tumors are diagnosed using T1-weighted, contrast-enhanced magnetic resonance imaging (CE-MRI). Semantic gaps between MRI image's lower/higher level visual information observed manually present primary difficulties for CBIR systems. Handcrafted features are used in traditional feature extractions to close this gap, but only low- or high-level features are taken into account. To narrow gaps without relying on hand-crafted features, feature extractions that combines/encodes low- and high-level features must be developed where DL methods are effective in feature representations. They can include the feature extraction step into self-learning and completely represent both high/low level data. Consequently, a novel approach for feature extractions utilizing deep convolutional neural networks (VGG19) with closed metric learning gauge similarity degrees between database and query images. To improve retrieval performances, additionally transfer learning and fine tuning of blocks were employed. To narrow this gap without relying on hand-crafted features, developing feature extractions that combine/encode low/high-level features are pertinent. When it comes to feature representation, DL methods are effective as they represent both high and low-level data and include feature extractions by self-learning.

Sudhish et al [22] presented CBIR pipelines that use CNNs in extracting features and clustering for feature map indices. The work reduced dimensionalities of previously generated feature vectors with gain based multi-level feature selections. Their experiments used 5-fold cross-validations on BraTS 2018 and 2020 datasets MRI brain image retrieval performances attained by their suggested system for mean average Precision values of 98.15% and Precision@10 values of 97.62% respectively were obtained. Their results supported therapeutic relevance and effectiveness of their suggested approach.

Owais et al [23] presented an improved residual networks (ResNet), a solution based on artificial intelligences for classifying medical images generated from multiple modalities. Their experiments employed 12 datasets spanning 50 classes where their strategy obtained higher accuracy and F1.scores (81.51% and 82.42%) respectively while CBMIR method in comparison achieved 69.71% and 69.63% respectively.

Chethan et al [24] suggested usage of Local Ternary Patterns (LTP), Histogram of Oriented Gradients (HOG), and Tamura feature extraction techniques. The characteristics of medical images were retrieved and used to classify and retrieve brain tumor images using Deep Neural Networks (DNN). Subsequently, an infinite feature selection (Inf-FS) approach with sparse auto encoders based DNN selected best features from feature vectors, resulting in enhanced classifications. Additionally, their suggested strategy's retrieval performances were improved by Euclidean Distances when evaluated using data from Contrast Enhanced Magnetic Resonance Image (CE-MRI) and the Open Access Series of Imaging Studies (OASIS). Their DNN classifications with sparse auto encoder improved sensitivity, specificity, and error rate values while achieving an overall accuracy of 95.34% (OASIS) and 99.87% (CEMRI) datasets. Average Retrieval Precision (ARP) is used to gauge the suggested strategy's retrieval performance, and it is contrasted with two current methods: Local Mesh Vector Co-occurrence Pattern (LMVCoP) and CBIR-based Convolutional Neural Network (CBIR-CNN). The suggested strategy has a high ARP of 98.33% and 88.25%, respectively on CE-MRI and OASIS datasets when compared to CBIR-CNN and LMVCoP methods. Applications for medical image retrievals employ DNN-based nonlinear feature data categorizations and suitable feature selections based on Inf-FS.

Ahmed et al [25] found that the method of pre-training massive amounts of image data from thousands of distinct classes results in pre-trained After training, CNN models and the information may be easily shared. Many useful pre-trained CNN models are in use in the domains of object recognition, image classification, and medical image retrieval. Offline features were extracted precisely using pre-trained CNN models, ResNet18 and SqueezeNet with CBMIR based image retrievals. The medical datasets tested in this work were PH2 and Kvasir which showed that their suggested technique achieved better results. The suggested performed better than other methods with precision of 97.75% and 83.33% respectively in retrieval assessments for Kvasir and PH2 medical image datasets, ,.

PerumalSankar et al [26] optimized In order to get optimal outcomes and increased accuracy, MRI image feature extractions and retrievals are performed using Edge-based GLCM (EGLCM) and artificial bee colonies (ABC) based artificial neural networks (ANNs). Pre-processes, feature extractions, optimal

retrievals utilizing ABC-based ANNs, and GLCM were four crucial phases of the proposed study. To ascertain textural attributes including homogeneity, energy, correlation, and contrast, GLCM creates a co-occurrence matrix. A feature vector consisting of eight properties is used to represent images. Next, to improve retrieval performance, we combine ABC-based ANN with association rule mining. We do this by employing 1000 and 100 MRI images for the training and validation stages, respectively.

Qayyum et al [27] created DL framework for medical CNIR utilizing CNNs. Their networks were using an intermodal dataset with 24 classes and five modalities. Medical images were retrieved using categorization findings and learnt characteristics. The best retrieval outcomes occurred by using class-based predictions. Their approach worked best for retrieving multimodal medical images of various bodily parts where for retrieval tasks, average precisions of 0.69 and average classification accuracies of 99.77% were obtained..

Ayyachamy et al [28] suggested a CBIR framework that makes use of deep CNNs to retrieve medical images. They reported medical image retrievals using pre-trained neural networks i.e. ResNet-18,. They demonstrated their strategy using multimodal datasets with four modalities (PET, CT, MRI, MG, and CT) and twenty-three classifications. The study achieved average precisions of 0.90 and average classification accuracies of 92% in retrievals. Their suggested approach can help with radiologist training and clinical diagnosis.

Nair et al [29] suggested a retrieval mechanism that is effective and includes four features: First, the input image is pre-processed and Canonical correlation analysis is utilized to extract characteristics (CCA). This process was used to extract the feature and perform a detailed analysis in the pixel and feature domains. Secondly, applied Fuzzy C describes how pixel intensity data is arranged into characteristics using singular value decomposition. This makes it possible to arrange the image according to each pixel's intensity value. The third approach is a deep CNN using SVM classifier, which is easy to design and simply requires minimal feature vector representations of database images to be retained, as well as class levels at which they must be retrieved. Lastly, the performance was assessed using the following metrics: accuracy, correct rate (CR), error rate (ER), and mean average precision. The medical images in a database are retrieved using the classification findings and learning characteristics. The suggested retrieval system outperformed conventional method by 95.9%, 94.96%, 95.37%, and 95.798%, for obtained average values of precisions, recalls, f-measures, and accuracies respectively.

3. Proposed Methodology

This research work suggests ensemble DL based classifications and retrievals for MRI brain tumor images using content-based methods. In the initial stage, an EBF is used which is an improved version of the bilateral filter used in image processing to preserve edges while reducing noise. Then the image Normalization process is carried out using IWCDF. Following this stage, the tumor portion is identified by applying the Watershed Segmentation method to segment the images. After that, EWOA is used to extract the features. The enhanced cuckoo search (ICSA) algorithm is then used to carry out the feature selection. At the indexing step, the R*-tree approach is used to improve search efficiency, and Mahalanobis Distance with relevance feedback is used to compute the similarity measure during that phase. Lastly, a brain tumor diagnosis using the EDL model is suggested.

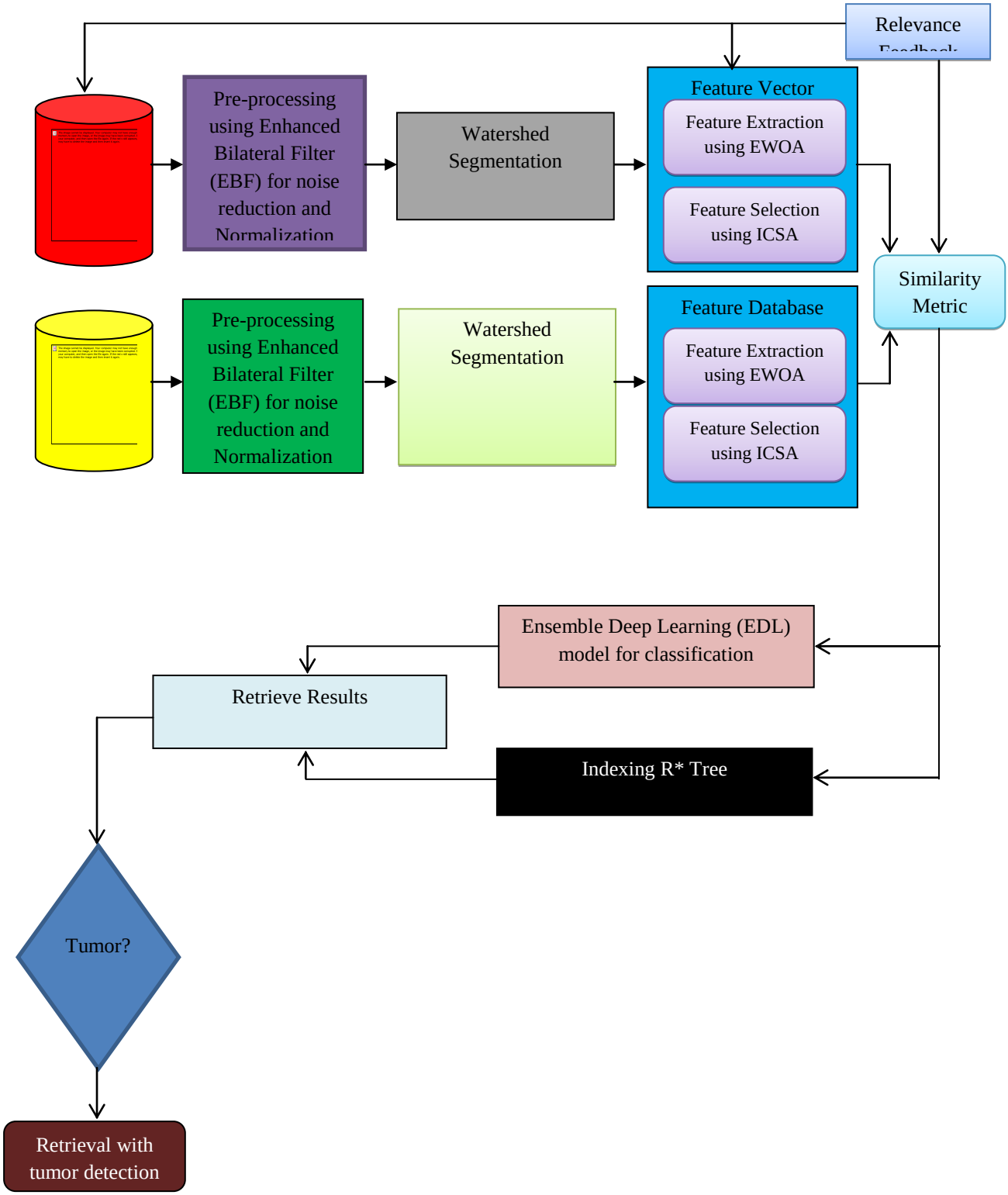

Figure 1: Proposed Methodology Diagram

3.1. Prerpocessing using EBF

Preprocessing is the process of eliminating extraneous noise from imagegraphs, or de-noising them. Smoothing is a type of preprocessing that softly blurs images without changing boundaries [23]. Even though the dataset utilized for this technique came from a website that could contain noise, images produced by modern MRI equipment could be more accurate. Images conveyed via electronic sources may be impacted by noise. In this preprocessing step, the MRI images are denied illumination after normalizing to ensure consistency in intensity/gray level. The EBF is applied to either enhance or modify the image. The EBF is an improved version of the bilateral filter used in image processing to preserve

edges while reducing noise. It addresses the limitations of traditional filtering techniques, which often blur edges along with noise reduction. The enhanced bilateral filter combines both domain (spatial) and range (intensity) filtering, but with optimized functions for preserving details in complex images.
The bilateral filter works by weighting pixel values based on both the spatial distance (how far apart the pixels are) and the intensity difference (how different their pixel values are). It effectively smooths similar regions while preserving edges, as sharp intensity changes are less likely to be averaged.
The standard bilateral filter is defined by:

$$I_{BF}(x) = \frac{1}{w(x)} \sum_{y \in S} I(y).\, f_s(\|x - y\|).\, f_r(\|I(x) - I(y)\|) \quad (1)$$

- $I_{BF}(x)$is the filtered intensity at pixel x.
- $I(y)$is the intensity of pixel y in the neighborhood S.
- $f_s(\|x - y\|)$are spatial (domain) kernels that reduce influences of distant pixels.
- $f_r(\|I(x) - I(y)\|)$arerange kernels that reduces influences of pixels with different intensities.
- $w(x)$is a normalizing factor to ensure the sum of the weights equals 1.

The Enhanced Bilateral Filter builds upon this by modifying either the spatial or the range kernel to further improve edge preservation, or by adapting the filter for specific types of noise or image features.
Enhanced Bilateral Filters can be mathematically depicted as:

$$I_{EBF}(x) = \frac{1}{w(x)} \sum_{y \in S} I(y).\, g_s(\|x - y\|).\, g_r(\|I(x) - I(y)\|) \quad (2)$$

- $g_s(\|x - y\|)$is the enhanced spatial kernel, which may be modified to have a sharper drop-off function.
- $g_r(\|I(x) - I(y)\|)$is the enhanced range kernel, which is more sensitive to intensity variations near edges.

Hence it is refined control over noise reduction and edge preservation compared to traditional methods, making it highly effective for MRI images.

3.2. Image Normalization using IWCDF

Here the MRI images are normalized using IWCDF. Normalization using the Weibull Cumulative Distribution Function (WCDF) is a technique employed in statistical analysis to scale or transform data values according to the Weibull distribution's characteristics. Because the Weibull distribution may be used to simulate a wide variety of data sources, it is frequently employed in reliability engineering, failure analysis, and life data analysis.
An improved form of the Weibull Cumulative Distribution Function (WCDF) generally involves modifications to the traditional Weibull CDF to better suit specific applications or datasets. These improvements aim to enhance the accuracy of MRI image. The formula remains largely similar to the standard WCDF, but with dynamically estimated parameters. It is

$$F(x) = 1 - \exp\left(-\left(\frac{x}{\lambda(t)}\right)^{\beta(t)}\right) \quad (3)$$

Where $\lambda(t)$ and $\beta(t)$are functions of time or other factors to adapt to changing data trends.
The ultimate results of pre-processed images are displayed in Fig.2 (b) with MRI image inputs in Fig.2 (a).

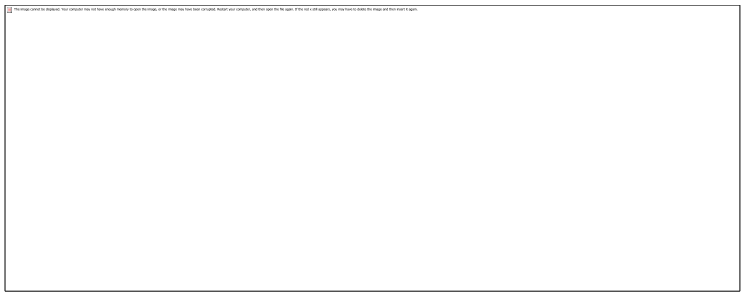

Fig 2. (a) Input MRI (b) Image Preprocessing Result (C) Object boundaries by applying watershed transform

3.3. Watershed Segmentation based Image segmentations

WaterShed Segmentation (WSS) is one gradient-based segmentation method. It views images' sgradient maps as relief maps and images are divided assuming they are dams where divided regions are referred to as catchment basins. WSS solves several image segmentation problems. It is recommended for imagegraphs with a greater intensity value. The primary cause of WSS is over segmentation. To control over segmentation, marker-controlled WSS is used. One useful use of the Sobel operator is edge detection

(ED). In marker controlled WSS, the edge of the object is identified via Sobel operators where Sobel matrices are depicted in Equation (4):

$$M_X = \begin{bmatrix} -1 & -2 & -1 \\ 0 & 0 & 0 \\ 1 & 2 & 1 \end{bmatrix}, \quad M_Y = \begin{bmatrix} -1 & 0 & 1 \\ -2 & 0 & 0 \\ -1 & 0 & 2 \end{bmatrix} \qquad (4)$$

The equation for , the Gradient Magnitude (GM) in marker-controlled WSS is depicted below:

$$M = \sqrt{{M_X}^2 + {M_Y}^2} \qquad (5)$$

$$\text{Angle}, \theta = \tan^{-1} \frac{M_Y}{M_X} \qquad (6)$$

3.4. Feature Extraction using EWOA

EWO extracts features in this work. Finding pertinent features from the ASD data to distinguish between ASD and non-ASD features is the purpose of feature selection. For many optimization issues, the WOA is utilized to choose pertinent attributes and determine the best solution. WOA method concentrated on choosing pertinent characteristics and demonstrated that its effectiveness may be modified to yield superior outcomes. WOA is utilized for selecting features in ASD datasets for accurate categorization.

Humpback whale hunting tactics and the development of an equation for those tactics served as the inspiration for the WOA approach. The whales hunt using a bubble-net approach, circling and feeding on their food, which is mostly tiny fish. Deep below the fish, whales emerge and begin to surface, forming a large ring of bubbles. The fish are compelled to surface by the bubbles acting as a trap. Whales pursue fish that are rising to the surface Jin et al, (2021) [30]. There are three steps to the hunting process in theory: exploitations, circling, and explorations where explorations dictate the quality of fishes consumed. Phase of encirclement: Whales locate the fish and encircle them. The ideal location's starting point is initially undefined and chosen at random. Other agents update their positions in response to the random initiations, and revised positions become best places to reach targets.

The variation of individuals is decreased during the WOA exploitation phase since it merely mimics and learns from the actions of the present best solution. The process of learning from random individuals during the WOA's exploration phase suffers from some blindness and ineffective information flow between groups, which has an impact on the method's pace of convergence. Therefore, the poor convergence speed of the conventional WOA is problematic. EWOA is suggested as a solution to the aforementioned issue in order to accelerate convergence.

In animal swarms, individuals gain knowledge from both neighbouring members which can significantly enhance personal qualities. Adaptive social learning technique forms neighbourhoods by determining social ranking, social impacts, and social networks which is used to build whales' adaptive neighbourhoods and enhance connections amongst groups. A novel strategy utilizing neighbourhood updates is created to increase population diversity while preserving computation accuracy.

Equations (7) and (8) can be used to depict the location of the whale and the surrounding area.

$$\vec{H} = |\vec{C}x\vec{X} * (t) - \vec{X}(t)| \qquad (7)$$

$$\vec{X}(t+1) = \vec{X}(t) - \vec{A} \times \vec{H} \qquad (8)$$

$\vec{A}$and $\vec{C}$imply vector coefficients obtained using equations (9) and (10), t signifies current iterations, phrase $\vec{X}$provides positional vectors and $\vec{X} *$ stands for arbitrary answers began arbitrarily.

$$\vec{A} = 2\vec{a} \times \vec{r} - \vec{a} \qquad (9)$$

$$\vec{C} = 2x\vec{r} \qquad (10)$$

Each time through an iteration, the elements of $\vec{a}$ are reduced linearly from 2 to 0, representing a random number from 0 to 1.

Bubble-net techniques are used by humpback whales for hunting by circling their preys**.** Whales enclose their prey, which includes fishes, and then modify their locations to choose best courses of actions. Equations (11) and (12) reveal the WOA's primary math component.

$$X(t+1) = X^*(t) - A.|C.X^*(t) - X(t)| \text{ if } p < 0.5 \qquad (11)$$

$$X(t+1)|C.X^*(t) - X(t)|.e^{bl} \cos(2\pi t) + X^*(t) \text{ if } p \geq 0.5 \qquad (12)$$

heret stands for time or iteration indices, X represents vectors of whale positions, and X* stands for obtained ideal solutions; A=2a. (r-a); C=2.r; r imply random vectors with values ranging from 0 to 1; b stands for constant values based on specific paths, determines form of logarithmic spirals where in this work, its value is 1; a stands for coefficient vectors that reduce linearly from 2 to 0 on iterations.; The random number l is in the range of -1 to 1. When updating the positions of the whales, p, a random value from 0 to 1, is utilized to alternate among (11) and (12); in Eqs. (13) and (14), given that the probabilities are 50% and 50%, whales have an equal probability of randomly choosing either course through the optimization stage. The random value of vector A is [- 1, 1] when in the bubble-net stage, but it can be more or less than 1 within the searching stage. The method of searching is illustrated in Equation (13)

$X(t+1) = X_{rand} - A.|C.X_{rand} - X(t)|$ (13)

The WOA method is enforced to conduct a worldwide search by this random search system, which prioritizes the searching process when the value of |A| is bigger than one. The WOA searching method starts with the creation of random solutions. Subsequently, the method presented in Table 1 is employed to update these solutions repeatedly. Searches continue until a pre-determined max. iterations are reached.

Exploitation phases:This phase involves two stages (i) surrounding, and ii) spirally updating positions. One way to define encircling behaviours is to decrease$\vec{a}$ linearly from 2 to 0 for each iteration. Revise the spiral's position: The whale's helical movement and relationship to the fish are determined by

$\vec{X}(t+1) = \vec{D}xe^{b1}xcos(2\pi l) + \vec{X}*(t)$ (14)

Here $\overrightarrow{D'} = |\vec{X}*(t)\_\vec{X}(t)|$ is the present distance among the whale and the fish, b an immovable element that symbolizes the whales' spiral motion, and b random vectors of $[-1,1]$. Furthermore, there is an option: deep plunges by circling and building spirals, given as equation 11, or randomize vector values of p in the interval [0,1].

Exploration phase:Whales look for fish that are rising to the top as part of a global fish exploration effort. $\vec{A}$, implies values of vectors in the interval [0,1] (0 denotes explorations and 1 denotes exploitations) serve as the basis for decisions to alternate between exploitations and explorations. And the equations (15) and (16) indicate the whale's new location.

$\vec{H} = |\vec{C}x\vec{X}_{rand} - \vec{X}|$ (15)

$\vec{X}(t+1) = \vec{X}_{rand} - \vec{A}x\vec{H}$ (16)

Where $\vec{X}_{rand}$ provides whales' new locations selected randomly from remaining whales.

Adaptive social learning strategy

By building neighbourhood memberships for every whale based on social learning theory, information sharing amongst groups can be enhanced altering imitating present best solutions, and increasing method's capacity to deviate from local optimal solutions in the populations.

$G(t) = \{x_1(t), x_2(t), \dots, x_N(t)\}$ (17)

Here N implies size of the population. To create sorted population, fitness of persons are determined and ranked in an ascending order.

$G_1(t) = \{x_{(1)}(t), x_{(2)}(t), \dots, x_{(N)}(t)\}$ (18)

and social ranks of $x_{(i)}(t)$ are:

$I_{(i)}(t) = \frac{R_{(i)}(t)}{N} i = 1,2,\dots,N$ (19)

Where $R_{(i)}$ implies random numbers and $I_{(i)}(t)$stands for person's relationship with another person.

Hence, the technique's exploitation phase primarily focuses on finding an ideal solution, while group cooperation allows for exploration. A unique whale search approach defined by adaptive social neighbourhood approach is developed.

Algorithm 1: EWOA

Input: MRI dataset

Output: Extracted features

```
Begin
establish the whale population's positionsX (ASD dataset)
determine each whale's fitness (feature)
set a and r, compute A and C
set X* to be  top hunter whales' positions
sett= 1
whilet ≤ max iterations do
for hunting whales do
ifp < 0.5
if |A| < 1
change locations of hunting whales with (11)
else if |A| ≥ 1
Choose other search agents arbitrarily
update locations of unting whales with (12)
end if
else if p ≥ 0.5
update current hunting whale positions with (13)
end if
calculate local ideal solutions with (17) & (18)
update exploitations with (19)
end for
update X* on finding improved solutions
t = t +1
end while
```

EWOA is employed by the suggested system to identify feature combinations that optimize classification accuracy while minimal chosen autistic features. Locating the ideal location in the search space that optimizes the specified fitness function needs intelligence because the feature space has each feature assigned a separate dimension, and the span of each dimension varies. Considering the autism training data, the EWOA's fitness function attempts to optimize its classification accuracy over the validation set.

3.5. Feature selection using Improved Cuckoo Search algorithm (ICSA)

Because certain cuckoo species parasitize other birds' nests by depositing their eggs there, cuckoo search (CS) method Optimizations are based on this knowledge. The host birds either reject the alien eggs or abandon their nests to construct new ones when they realize the eggs are not their own. The CS algorithm makes use of this tendency, wherein eggs inside nests indicate potential solutions, while cuckoo eggs represent novel solutions. The less-than-ideal option in the nest is replaced if the new solution performs better.

Each nest in the most basic version of Cuckoo search has a single egg. New solutions are created via Levy flights. The guidelines adhered for CS are:

One egg is laid in a randomly selected nest by each cuckoo as it breeds one at a time. The finest nests, which provide superior eggs, will be inherited by subsequent generations. Viable host nest counts are fixed, and hosts positively identify alien eggs [0, 1] where host birds have two choices: either rejecting the eggs or leaving nests and to build new ones elsewhere.

Premature convergence is the primary issue with the current setup. The disadvantage stems from the Cuckoo search algorithm's stalling. Hybridization techniques are used to modify the algorithm to create an improved cuckoo search. This suggested technique also improves the global search space.
Every nest in the suggested method holds several eggs. The cuckoo is chosen at random after the halting requirements are satisfied. The cuckoo's kind is verified. Eggs from European cuckoos are created using mutation operators that use any eggs in nests; for common cuckoos, the best eggs are chosen using the levy flying procedure. If the egg's kind is unknown, a random egg is created using a cryptic solution and its fitness value is calculated. The weakest egg in each nest is randomly selected, and a nest is picked.The relevant eggs' fitness roles are contrasted. The best response replaces the weakest egg in the nest. The nest's top solutions are counted and assessed. Only the best solutions survive in their nests, while the poorest are discarded. Nests are sorted by best replies, and the best current solutions are recognized. The proposed system's algorithm is as follows.

Pseudo Code for EWOA

```
Generate populations of n host nests with m eggs;
While (t<MaxGenerations) or (stop criteria) for nests
Randomly obtain cuckoo types (say, i);
Examine types of cuckoos
If cuckoo_type = Common_cuckoo
Use Levy flights to generate best eggs in nests;
Else if cuckoo_type = European_cuckoo
Use  Levy flights to generate eggs with uniform mutations
Operators with any eggs in nests;
Else
Create eggs with random solutions (cryptic eggs)
Evaluate their fitness Fi
Select  eggs with worst solutions in nests (say, j);
If (Fi <Fj)
Modify j using new solutions i;
End if
Rank eggs based on solutions;
Identify best solutions (amongst eggs) in nests;
Abandon fractions (pa) of eggs in nests which have
Worse solutions and build  new solutions using Levy flights keeping best
solutions;
End for
Rank nests' eggs using fitness values and find current bests;
End while.
```

3.6. Similarity and Indexing Schemes

CBIR systems often calculate a QI visual similarity and images stored in a database. It has become common practice recently to create a variety of similarity metrics for IR by empirically estimating feature distributions where multiple distance measurements influence IR system's retrievals substantially. This section covers some commonly used indexing and similarity techniques.

Indexing

Main issues with CBIR systems stem from efficient indexing as image feature vectors (FV) have large dimensions making them inappropriate for traditional indexes. Dimensionality reductions (DR) are usually carried out before creating functional indexing systems. IBA is thus utilized in this case to achieve this. After DR, the multi-dimensional data are indexed. By ranking each image according to how similar it is to the others, indexing is a sorting technique. It is useful in increasing query performance throughout the search process and makes a substantial contribution to the effective retrieval of image sequences [26]. A decent index helps make searching simple and efficient. To this end, in this paper, the R*-tree technique has been proposed.
By using improved insertion and splitting algorithms to reduce overlaps in the leaf nodes, the R*-tree achieves superior query speed while maintaining a similar tree topology to the R-tree [31]. Fig. 3 is an illustration of a R*-tree.

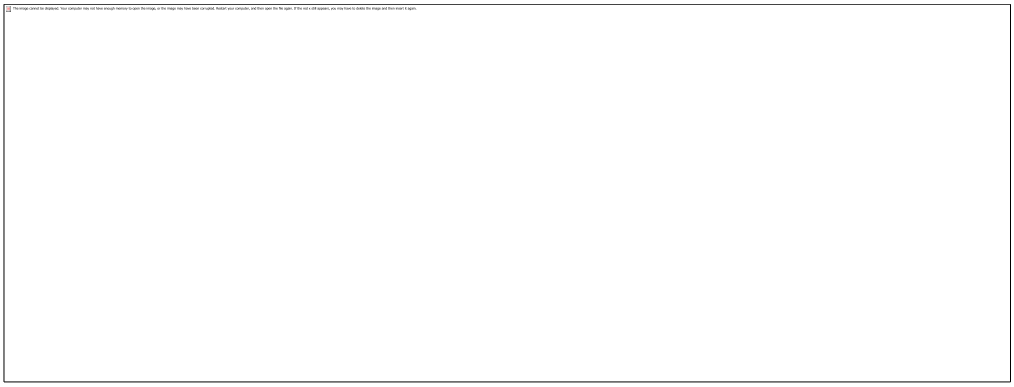

Fig 3: An image of R*-tree

3.7. Relevance Feedbacks

Image similarities are task related, subjective, and materialistic in human minds. For IR, content-based methods are often reliable. Retrieval results based merely on similarity of visual characteristics do not necessarily guarantee significance in a perceptual or semantic sense.

Additionally, each feature tries to capture only one portion of an image characteristic. Users generally struggle to explain exactly how different aspects relate to one another. To address this issue, interactive relevance feedback—a technique used in conventional TB information retrieval systems—was developed. Relevance feedback is one type of supervised active learning technique that may be used to improve information system performance. The idea is to leverage both good and negative user examples to enhance system performances

For given queries, systems initially obtain lists of rated images based on predefined similarities or characteristics. The acquired images are annotated by the user with a note indicating whether or not they are relevant (+ve instances) to the query (-ve instances). The system will present the user with a new selection of images and enhance retrievals based on users' reactions. In relevant feedbacks, inclusions of both positive and negative cases are main issues in building queries and/or adjust similarity measure.

3.8. EDL model to classify brain tumor

Classification is the organized grouping of images that have been categorized under a certain category. The two processing steps that comprise categorization are training and testing. During the training phase, different data is generated and image features are separated. Those feature areas are used to classify the images. The input for the tumor categorization and identification method consists of certain characteristics. Long short-term memory networks (LSTM) and ensembles of fuzzy convolutional neural networks (FCNN) are employed in this work.

Fuzzy convolutional neural network: FCNN uses four layers to guarantee prediction accuracy while cutting down on calculations. Four CNN layers are used as shown in Figure 4: input, convolution, softmax and output layer.

(i) Input Layer: This layer is trained using neurons where N x k arevariate values of inputs and N represents data length.

(ii) Convolution Layer: Data from the preceding layer was twisted using convolution filters.

(iii) Pooling Layer: This reduces the sample size, the dimensionality, and the number of parameters, respectively. A single calculation is carried out, and it is a masking technique that is conducted on the input matrices using a sliding window that varies in size according to the convolution kernel. The fuzzy membership function is used in the computation of weight values.

(iv) Softmax or Fully Connected Layer: Activation functions provide outputs that are not linear by combining linear networks. A Softmax function is a squashing function that uses layers to provide probabilities for several classes.

(v) Output Layer: According to n feature classes, which are completely related to the feature layer, this layer generates neurons or nodes. To produce class labels from inputs in classification, the highest output neuron is chosen.

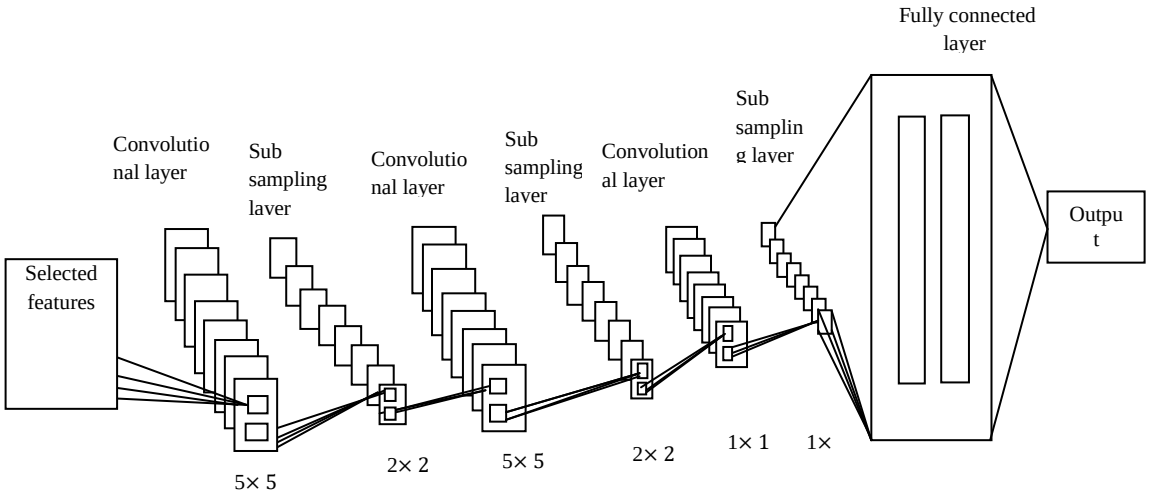

Figure 4: Convolutional Neural Network Architecture

Modified LSTM: Standard RNNs, the LSTM is an RNN architecture designed to more precisely imitate temporal sequences and their long-term interactions. Figure 5 depicts LSTM cells which include input, forget and output gates with component for activating cells. Cell activations are controlled by the use of specifically designed multipliers. They do this by receiving activation signals from a variety of various sources (Dai et al., 2019).

The input gates of LSTM are defined as

$$i_t = \sigma(W_{xi}x_t + W_{hi}h_{t-1} + W_{ci}c_{t-1} + b_i) \quad (20)$$

The forget gate is defined as

$$f_t = \sigma(W_{xf}x_t + W_{hf}h_{t-1} + W_{cf}c_{t-1} + b_f) \quad (21)$$

The cell gate is defined as

$$c_t = f_t c_{t-1} + i_c tanh(W_{xc}x_t + W_{hc}h_{t-1} \quad + b_c) \quad (22)$$

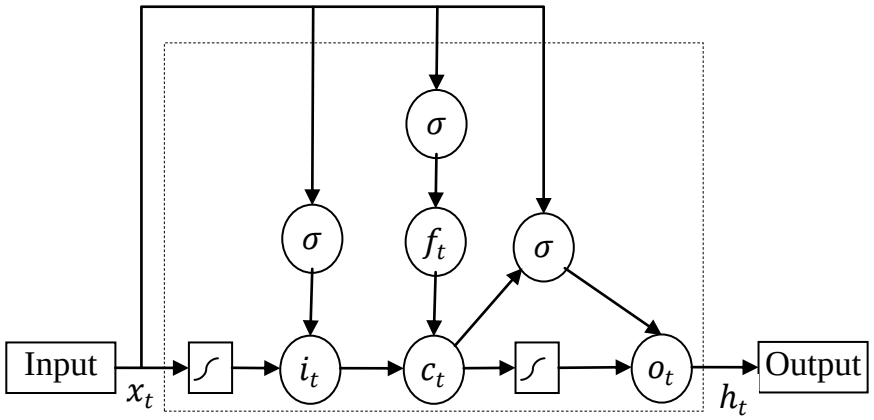

Figure 5: Long Short-Term Memory Cell

The output gate is defined as

$$o_t = \sigma\left(W_{x0}x_t + W_{h0}h_{t-1} + W_{c0}c_t \quad + b_0\right) \quad (23)$$

Ultimately hidden states are computed using

$$h_t = o_t tanh(c_t) \quad (24)$$

tanh represents hyperbolic tangent activations, x_t- implies inputs at times t while W and b stand for network's Weights and Biases respectively.

LSTM gates avoid data changes from the rest of networks and store it in in the memory cells with different time steps. LSTM networks propagate errors and hold onto signals far longer than ordinary RNNs. In order to circumvent these problems, the work that is being proposed uses modified long-term memory, which includes a weighted scheme that is based on weighted regression. According to this method, the relevance of each feature to the estimation point determines how much weight it is given to

in the overall scheme. Based on 3D distance metrics between observation and estimated estimate points, the weight corresponding to each characteristic may be established.
The weight function was discovered to have the following form

$$\omega = \begin{Bmatrix} (1-\left(\frac{d}{h}\right)^3)^3 \to if|d| \le h \\ 0 \to \text{if}|d| > h \end{Bmatrix} \quad (25)$$

Where,
ω - indicates weights,
d - denotes separations between measurement and observation points.
h - half window widths.
The σ I f, o, and c stand for input gate, forget gate, output gate, and cell state, respectively. Logistic sigmoid function. Weight matrices represent Wci, Wcf, and Wco for peephole connections. Information flows in LSTMs are controlled by three gates (I, f, and o). Input gates determine input ratios which influence determinations of cell states because of equation (20). The forget gate decides whether to retain information in memory and delete it by forwarding the previous memory ht1 or not. Equation (22) was employed in the computation of the prior memory ratio, as well as equation (21). The output gate controls whether a memory cell's output is passed or not and depicted in equation (23). LSTM's three gates assist in handling vanishing and exploding gradient issues. Recurrent hidden layers are swapped with LSTM cells in LSTM-RNN architectures. Lung cancer categorization is provided via the output gate.

Ensemble learning using majority voting

A decision-making process called the Majority Voting (MV) uses classifiers that have been run n times, each time with increased power. Let us consider χ a set of N examples and C a set of Q classes. Definition of an algorithm set S = $\{A_1, A_2, A_M\}$ This includes the M classifiers that were utilized in the vote. Each instance x ∈ χ has been given one of the Q classifications. Every time a classifier runs, a prediction for every example is made. Each sample is given a final class that corresponds to the class that most classifiers predicted it would belong to. Each vote in MV is weighted according to the classifier's prediction accuracy value, abbreviated as Acc. Therefore, the total number of votes for class c_k may be expressed as follows:

$$T_k = \sum_{l=1}^{M} Acc\ (A_l) \times F_k(c_l) \quad (26)$$

$$F_k(c_l) = \begin{cases} 1 & c_l = c_k \\ 0 & c_l \neq c_k \end{cases}$$

where c_l and c_k are the classes of C. It is decided on which class has the highest overall weight. To identify the data as positive or negative, the classifiers are typically trained on several independent training sets with weights applied.

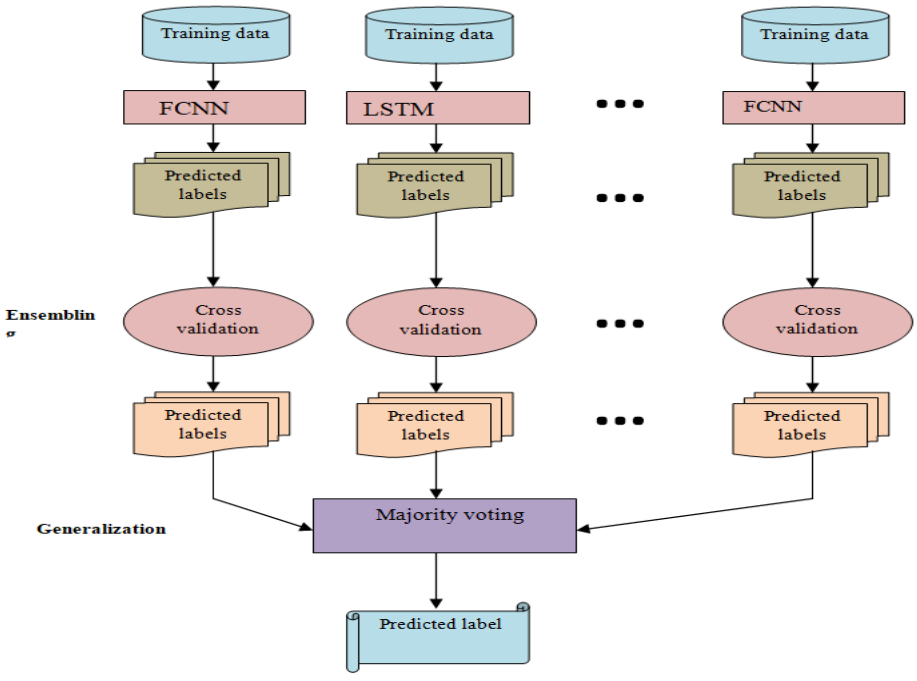

Figure 6: EDL Approach

RESULTS AND DISCUSSION

The experimental findings of three algorithms on IBSR dataset (http://www.cma.mgh.harvard.edu/ibsr/) which has many image scans of patients with or without brain tumors are analyzed where query judgments on image categories are provided for objective performance measures [22]. The evaluation parameter is Average Precision, which is defined as the average ratio of total returned images to relevant images. The category that is first selected at random from the database in the experiments is assumed to be the target category for the user's query. The system then uses relevant feedbacks to improve the retrieval results. Ten examples are selected from the database and labelled as positive or negative in iterations of relevance feedbacks depending on database's ground truths..

The studies assessed the usefulness of numerous techniques for predicting ASD data using a variety of parameters often used in binary classification. Establish the true positive (TP), false positive (FP), true negative (TN), and false negative (FN) rates before calculating any performance metrics. The percentage of pertinent recovered occurrences, or precision, was the first performance metric. The second performance metric was recall, which represents the proportion of relevant events successfully retrieved. Accuracy and recall metrics are critical for determining the effectiveness of a prediction strategy, even if they are usually contradicting. Consequently, the F-measure, a single metric, may be created by combining these two measures with equal weights. Accuracies which are percentages of accurately predicted instances to all anticipated instances are final computed performance statistics.

Precisions are defined as ratios of correctly found positive observations to total expected positive observations.

$$Precision = TP/(TP + FP) \quad (27)$$

Sensitivities or Recalls are defined as ratios of correctly identified positive observations to total observations.

$$Recall = TP/(TP + FN) \quad (28)$$

F – measures are weighed averages of Precisions and Recalls and hence consider false positives and false negatives.

$$F - measure = 2 * (Recall * Precision)/(Recall + Precision) \quad (29)$$

Accuracies computed in terms of positives and negatives are as follows:

$$Accuracy = (TP + FP)/(TP + TN + FP + FN) \quad (30)$$

Specificity and sensitivity determine the percentage of tumor pixels properly identified to non-tumor pixels. Tumour pixel accuracies are ratios of identified and categorized pixels.

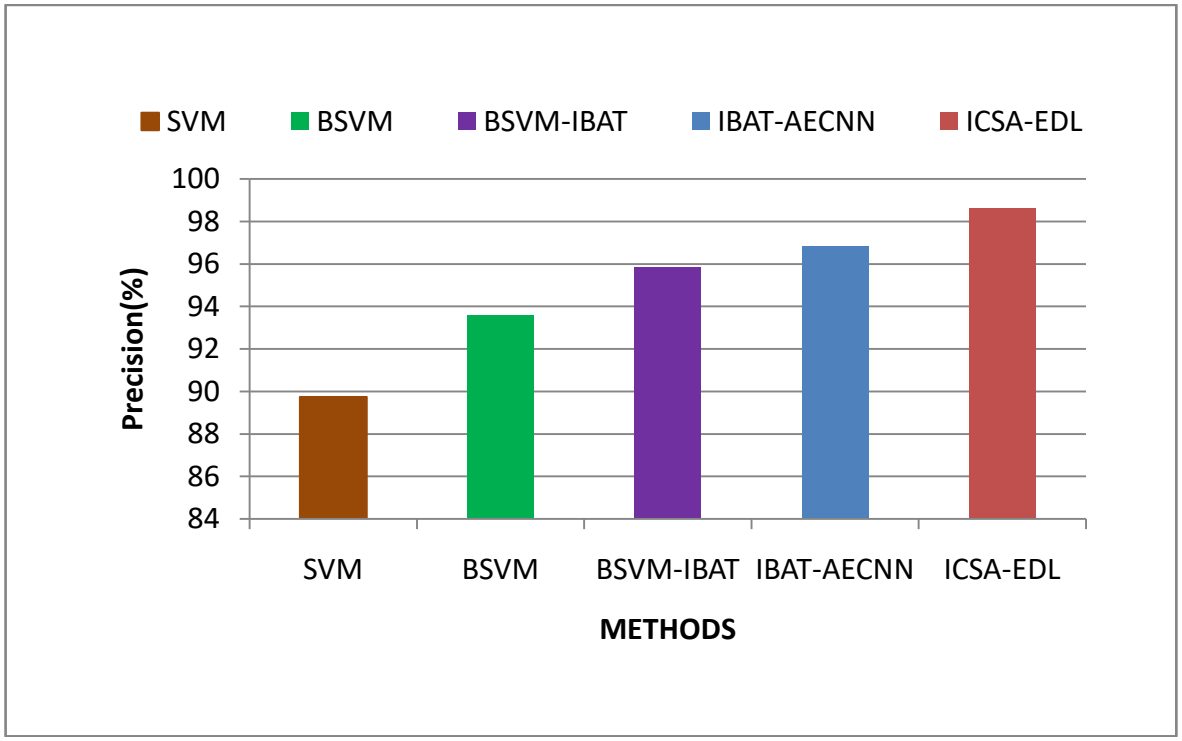

Figure 7: Results of the proposed and existing approaches' precise comparison

Figure 7 shows the proposed and current approaches' accuracy performance. The results demonstrate that feature extraction using EWOA and ICSA is effective for brain tumor classification. Additionally, the

suggested EWOA demonstrates that the effectiveness of linear transformations is mostly unaffected by the number of usable characteristics. This is a valuable characteristic, as it reduces the need for extensive tuning of the regularization parameter in the classifier. The proposed EWOA and ICSO has highly effective technique for solving the classification problem.

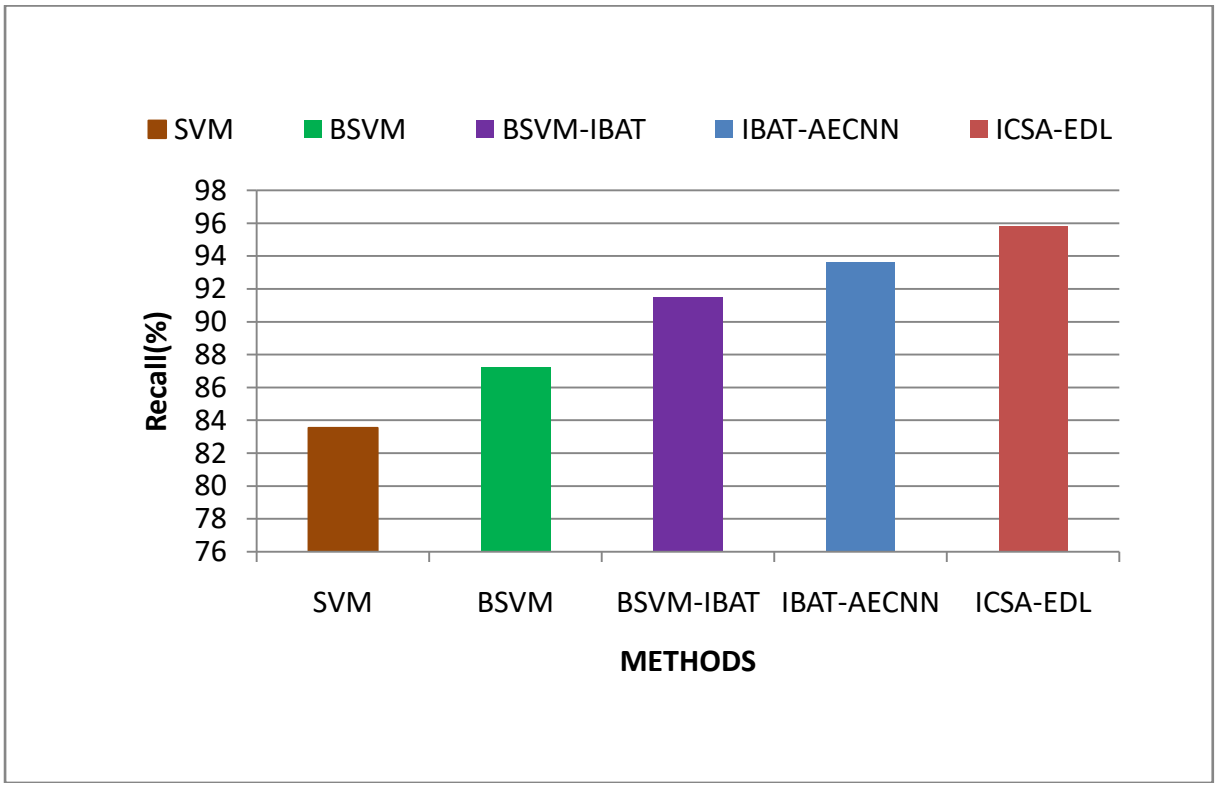

Figure 8: Recall comparison results of the proposed and existing methods

Figure 8 displays the performance results of the proposed and existing methods. An ICSA-EDL is 95.83% recall rate was found using the suggested strategy, whereas the existing techniques show lower recall rates: the IBAT-AECNN method has 93.62%, the BSVM-IBAT method has 91.74%, the BSVM method has 89.68%, and the SVM method has 87.25%.

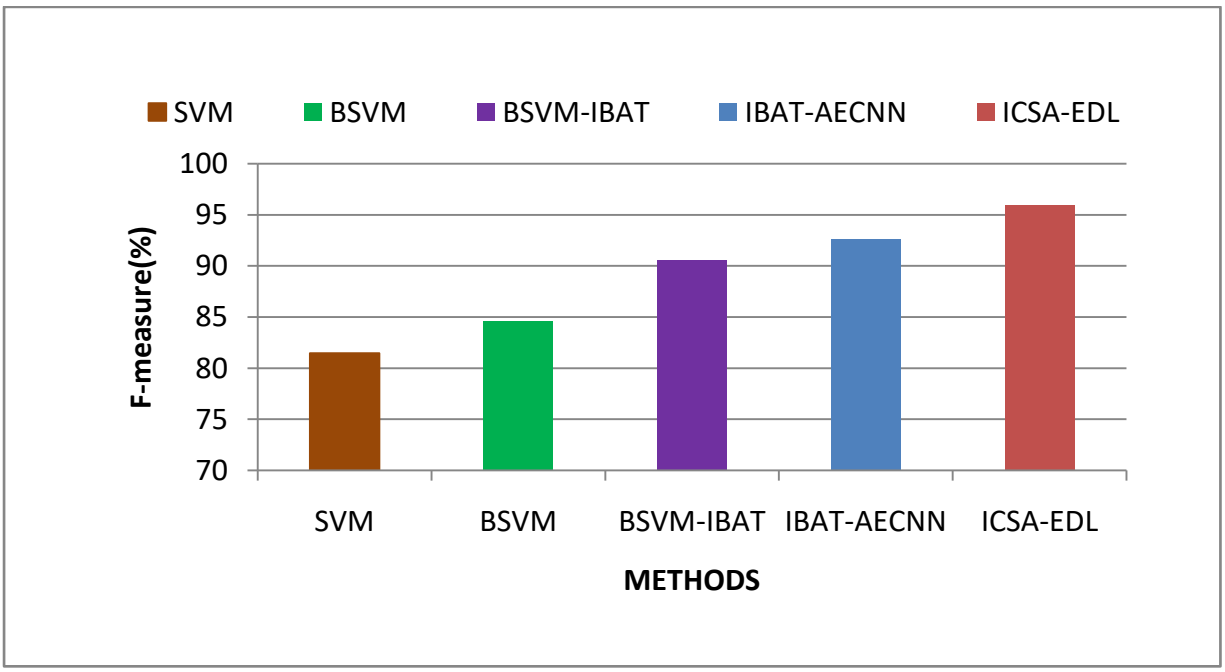

Figure 9: The proposed and current methods of F-measure comparative results

Figure 9 illustrates that the proposed ICSA-EDL demonstrates exceptional performance in disease prediction, significantly outperforming the BSVM-IBAT, BSVM, and SVM methods. The quantitative analysis, measured by the F-measure, aligns with the qualitative findings from ML assessments. Additionally, the proposed ICSA is compared with other advanced classification algorithms regarding their accuracy on the provided dataset.

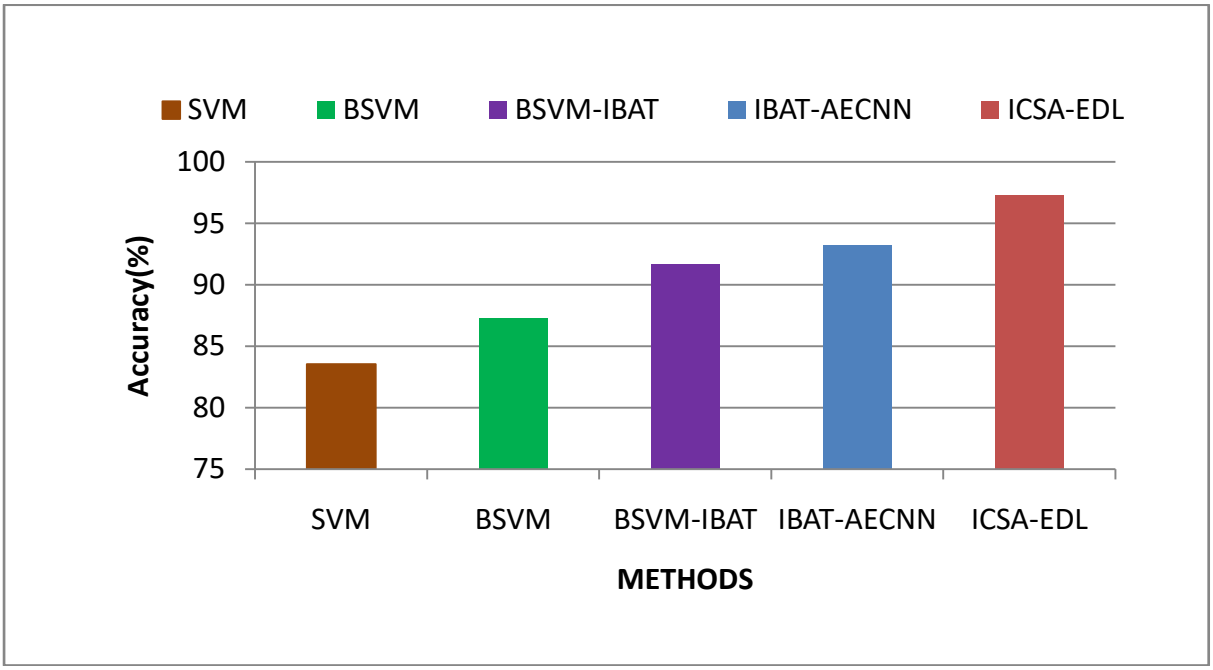

Figure 10: Comparison of the proposed and existing methods accuracy

Figure 10 shows the proposed method give more accuracy than the existing classifier. Likewise, all the mentioned classifiers, when applied to static data, perform poorly compared to the ICSA-EDL classifier. This highlights ICSA-EDL method's effectiveness in critical scenarios for brain tumor classifications. Hence, the accuracy of this classifier is higher compared to those built on previously established models.

CONCLUSION

This paper proposes CBIR system for MRI brain tumor images, based on ensemble DL. CBIR first chooses characteristics from a query or template image, computes a similarity measure, and then produces results by identifying tumors. Noise reduction, image normalization, and image preprocessing are done at this stage. Following this stage, the tumor portion is identified by applying the Watershed Segmentation method to segment the images. After that, EWOA is used to extract the features. The enhanced cuckoo search (ICSA) algorithm is then used to carry out the feature selection. At the indexing step, the R*-tree approach is used to improve search efficiency, and Mahalanobis Distance with relevance feedback is used to compute the similarity measure during that phase. Lastly, a brain tumor diagnosis using the EDL model is suggested. Lastly, a brain tumor diagnosis using the EDL model is suggested. Consequently, our classifier's accuracy is 97.8% greater than those based on previously validated models. A content-based approach for retrieving medical images was introduced by this effort. The study draws in light of the innovative solution that has been proposed and the concepts that have been looked at. Using an adaptive method, the program makes use of the similarities between query images and images stored in databases. A conceptually and computationally straightforward multi-resolution technique was given in the paper.

REFERENCES

[1] World Health Organization Cancer Fact Sheets. Available[online]: http://www.who.int/mediacentre/factsheets/fs297/en/index.html
[2] Stoitsis J, Valavanis I, Mougiakakou SG, Golemati S, Nikita A, Nikita KS (2006) Computer aided diagnosis based on medical image processing and artificial intelligence methods. NuclInstrum Methods Phys Res 569(2):591–595
[3] Yuan K, Feng S, Chen W, Jia S, Xiao P (2008) Diagnosis system of computer aided brain MRI using content based image retrieval. In: Proceedings of international conference on information technology and application in biomedicine, IEEE, pp 152–156

[4] Quellec G, Lambard M, Cazuguel G, Roux C, Cochener B (2011) Case retrieval in medical databases by fusing heterogeneous information. IEEE Trans Med Imaging 30(1):108–118
[5] Agarwal P, Sardana HK, Jindal G (2009) Content based medical image retrieval: theory, gaps and future directions. Graphics Vis Image Process 9(2):27–37
[6] Muller H, Michoux N, Bandon D, Geissbuhler A (2004) A review of content-based image retrieval systems in medical applications—clinical benefits and future directions. Int J Med Inf 73(1):1–23
[7] M. Huang, W. Yang, M. Yu, Z. Lu, Q. Feng, and W. Chen, ''Retrieval of brain tumors with region-specific bag-of-visual-words representations in contrast-enhanced MRI images,'' Comput. Math. Methods Med., vol. 2012, Oct. 2012, Art. no. 280538
[8] A. Shah, S. Conjeti, N. Navab, and A. Katouzian, ''Deeply learnt hashing forests for content based image retrieval in prostate MR images,'' Proc. SPIE, vol. 9784, p. 978414, Mar. 2016.
[9] J. Jiang, Y. Wu, M. Huang, W. Yang, W. Chen, and Q. Feng, ''3D brain tumor segmentation in multimodal MR images based on learning population- and patient-specific feature sets,'' Comput. Med. Imag. Graph., vol. 37, pp. 512–521, Oct./Dec. 2013
[10] M. Havaei et al., ''Brain tumor segmentation with deep neural networks,'' Med. Image Anal., vol. 35, pp. 18–31, Jan. 2017
[11] Y. LeCun, Y. Bengio, and G. Hinton, ''Deep learning,'' Nature, vol. 521, no. 7553, p. 436, 2015.
[12] D. Shen, G. Wu, and H.-I. Suk, ''Deep learning in medical image analysis,'' Annu. Rev. Biomed. Eng., vol. 19, pp. 221–248, Jun. 2017.
[13] F. Ciompi et al., ''Automatic classification of pulmonary peri-fissural nodules in computed tomography using an ensemble of 2D views and a convolutional neural network out-of-the-box,'' Med. Image Anal., vol. 26, no. 1, pp. 195–202, Dec. 2015.
[14] W. Zhang et al., ''Deep convolutional neural networks for multi-modality isointense infant brain image segmentation,'' NeuroImage, vol. 108, pp. 214–224, Mar. 2015
[15] H.-I. Suk, S.-W. Lee, and D. Shen, ''Hierarchical feature representation and multimodal fusion with deep learning for AD/MCI diagnosis,'' NeuroImage, vol. 101, pp. 569–582, Nov. 2014.
[16] H.-I. Suk, D. Shen, and Alzheimer's Disease Neuroimaging Initiative, ''Deep learning in diagnosis of brain disorders,'' in Recent Progress in Brain and Cognitive Engineering. Dordrecht, The Netherlands: Springer, 2015, pp. 203–213
[17] S. Pereira, A. Pinto, V. Alves, and C. A. Silva, ''Brain tumor segmentation using convolutional neural networks in MRI images,'' IEEE Trans. Med. Imag., vol. 35, no. 5, pp. 1240–1251, May 2016.
[18] D. C. Cireşan, A. Giusti, L. M. Gambardella, and J. Schmidhuber, ''Mitosis detection in breast cancer histology images with deep neural networks,'' in Proc. Int. Conf. Med. Image Comput. Comput.-Assist. Intervent., 2013, pp. 411–418.
[19] X. Liu, H. R. Tizhoosh, and J. Kofman, ''Generating binary tags for fast medical image retrieval based on convolutional nets and Radon transform,'' in Proc. Int. Joint Conf. Neural Netw. (IJCNN), Jul. 2016, pp. 2872–2878.
[20] Arakeri, M. P., & Ram Mohana Reddy, G. (2013). An intelligent content-based image retrieval system for clinical decision support in brain tumor diagnosis. International Journal of Multimedia Information Retrieval, 2, 175-188.
[21] Swati, Z. N. K., Zhao, Q., Kabir, M., Ali, F., Ali, Z., Ahmed, S., & Lu, J. (2019). Content-based brain tumor retrieval for MR images using transfer learning. IEEE Access, 7, 17809-17822.
[22] Sudhish, D. K., Nair, L. R., &Shailesh, S. (2024). Content-based image retrieval for medical diagnosis using fuzzy clustering and deep learning. Biomedical Signal Processing and Control, 88, 105620.
[23] Owais, M., Arsalan, M., Choi, J., & Park, K. R. (2019). Effective diagnosis and treatment through content-based medical image retrieval (CBMIR) by using artificial intelligence. Journal of clinical medicine, 8(4), 462.
[24] Chethan, K., &Bhandarkar, R. (2020). An Efficient Medical Image Retrieval and Classification using Deep Neural Network. Indian Journal of Science and Technology, 13(39), 4127-4141.
[25] Ahmed, A., Almagrabi, A. O., & Osman, A. H. (2022). Pre-trained convolution neural networks models for content-based medical image retrieval. Int. J. Adv. Appl. Sci., 9, 12.
[26] PerumalSankar, S., Vishwanath, N., &Jer Lang, H. (2017). An effective content based medical image retrieval by using ABC based artificial neural network (ANN). Current Medical Imaging, 13(3), 223-230.
[27] Qayyum, A., Anwar, S. M., Awais, M., &Majid, M. (2017). Medical image retrieval using deep convolutional neural network. Neurocomputing, 266, 8-20.
[28] Ayyachamy, S., Alex, V., Khened, M., &Krishnamurthi, G. (2019, March). Medical image retrieval using Resnet-18. In Medical imaging 2019: imaging informatics for healthcare, research, and applications (Vol. 10954, pp. 233-241). SPIE.

[29] Nair, L. R., Subramaniam, K., &Venkatesan, G. P. (2020). An effective image retrieval system using machine learning and fuzzy c-means clustering approach. Multimedia Tools and Applications, 79(15), 10123-10140.
[30] Jin, Qibing, ZhonghuaXu, and Wu Cai. "An Improved Whale Optimization Algorithm with Random Evolution and Special Reinforcement Dual-Operation Strategy Collaboration." Symmetry 13.2 (2021): 238
[31] Bechmann, N.,.Kriegel, H, Schneider, R. And Seeger, B. 1990, "The R* tree: An efficient and robust access method for points and rectangles", Proceedings of the SIGMOD, pp. 322–332.